Geomicrobiology Journal

ISSN: 0149-0451 (Print) 1521-0529 (Online) Journal homepage: http://www.tandfonline.com/loi/ugmb20

Nanosized Ferrihydrite Colloids Facilitate Microbial Iron Reduction under Flow Conditions

Julian Bosch , Andreas Fritzsche , Kai U. Totsche & Rainer U. Meckenstock

To cite this article: Julian Bosch , Andreas Fritzsche , Kai U. Totsche & Rainer U. Meckenstock (2010) Nanosized Ferrihydrite Colloids Facilitate Microbial Iron Reduction under Flow Conditions, Geomicrobiology Journal, 27:2, 123-129, DOI: 10.1080/01490450903456707

To link to this article: http://dx.doi.org/10.1080/01490450903456707

Published online: 17 Mar 2010.

Geomicrobiology Journal, 27:123–129, 2010

ISSN: 0149-0451 print / 1521-0529 online
DOI: 10.1080/01490450903456707

Taylor & Francis
Taylor & Francis Group

Nanosized Ferrihydrite Colloids Facilitate Microbial Iron Reduction under Flow Conditions

Julian Bosch,[1] Andreas Fritzsche,[2] Kai U. Totsche,[2] and Rainer U. Meckenstock[1,2]

[1]*Institute of Groundwater Ecology, HelmholtzZentrum München - German Research Center for Environmental Health, Neuherberg, Germany*

[2]*Institut für Geowissenschaften, Friedrich-Schiller Universität Jena, Jena, Germany*

Recent studies indicated that nanoparticulate minerals in the environment exhibit a higher reactivity than their respective bulk materials. Lately, this has also been reported for microbial iron reduction using nanosized iron oxides as electron acceptors. However, these results have been obtained under small-scale, static batch conditions. The study presented here implies a flow regime within porous medium under low salt conditions providing information on the retention of nanosized iron oxide and the long-term sustainability of their reduction. Goethite, present as coating on quartz sand as a default electron acceptor, was reduced by *Geobacter sulfurreducens* and discharged as Fe^{2+} up to a maximum concentration of 0.6 mM in the column effluent, finally representing 10% of the supplied ferric iron in total. Adding ferrihydrite colloids via the influent to goethite-coated quartz sand led to partial adsorption of the colloids, but also to a high reactivity with a maximum Fe^{2+} discharge of 1.2 mM. In total, 1.4 mmol out of 2.6 mmol ferrihydrite colloids were reduced. Upon addition of ferrihydrite colloids to the influent of a parallel column containing quartz sand without goethite coatings, the maximum concentration of discharged Fe^{2+} accounted also for 1.2 mM, and 0.4 mmol out of 0.6 mmol ferrihydrite colloids were reduced in total. The column experiments demonstrated that ferrihydrite colloids are highly reactive and bioavailable for microbial reduction under approximated in situ conditions.

Keywords advective flow, colloid, column experiment, Geobacter, iron hydroxide, iron reduction

Received 25 March 2009; accepted 1 October 2009.

Financial support was provided by the "Virtual Institute for Isotope Biogeochemistry" (VIBE) of the Helmholtz-Association, VH-VI-155, the DFG research unit FOR 580, and the EU-project "AQUAREHAB" (Grant agreement no.: 226565).

Address correspondence to Rainer U. Meckenstock, Institute of Groundwater Ecology, HelmholtzZentrum München - German Research Center for Environmental Health, Ingolstädter Landstr. 1, D-85764 Neuherberg, Germany. E-mail: rainer.meckenstock@helmholtz-muenchen.de

INTRODUCTION

The biogeochemical cycles of iron, manganese, sulfur, and other elements, have a strong impact on the environment. The reaction rates of the various involved abiotic and biotic processes determine turnover times and thus have a major impact on soils, groundwater, and the atmosphere. Mineral particles of nanometer size are especially reactive during many of the involved reactions, e.g., iron reduction. (Hochella et al. 2008). Nanosized mineral particles have a range of unique features causing this special behavior, e.g., a high specific surface area, higher interfacial energies, reactive surface structures dominated by defects and edgings, band gap changes and changes in redox behavior (Gilbert and Banfield 2005; Waychunas et al. 2005). Such minerals may occur in colloidal suspension under suitable conditions, e.g., low ionic strength of the medium. They may be highly mobile within the subsurface (Kretzschmar et al. 1995) and are abundant in nature (van der Zee 2003). The thermodynamic stability of iron (hydr)oxides in the environment as well as abiotic reduction rates of iron (hydr)oxides with hydroquinone have been shown to be dependent on particle size (Anschutz and Penn 2005).

In this study, we focus on the dissimilatory microbial reduction of nanosized iron (hydr)oxides under flow conditions. Microbial iron reduction is generally limited by the poor bioavailability of the immobile, crystalline Fe(III) as electron acceptor (Kerisit et al. 2007; Roden 1996). Recently, however, it has been revealed that nanosized hematite particles are highly reactive in microbial reduction (Yan et al. 2008; Bose et al. 2009). A systematic study of different iron (hydr)oxides in the nanometer range and in colloidal suspension revealed significantly enhanced reaction rates and bioavailability for nanosized particles as compared to their respective bulk materials (Bosch et al. 2010). In the latter study, a much higher intrinsic reactivity of colloidal iron oxides and a catalytic effect on the reduction of bulk aggregates was observed.

Earlier studies have demonstrated the effect of high reactivity induced by small particle size on reduction rates in batch incubations with cell suspensions (Yan et al. 2008). This included high

cell numbers and the absence of any adsorbing surfaces other than bacterial cells. Thus, artificial conditions were applied in comparison to environmental systems, e.g., aquifers. Aquafiers comprise heterogeneous, porous bulk phase materials, and distinct flow conditions within the pore spaces.

The present study therefore aims at demonstrating that ferrihydrite colloids also have an impact on microbial iron reduction rates under experimental conditions closer to environmental systems like water-saturated aquifers. This includes a goethite-coated matrix, realistic liquid/solid-ratios, low ionic strength of the aqueous medium, low initial cell density, and flow conditions. These conditions are known to affect the behavior of colloidal suspensions in terms of stability and mobility, so a similarly high reactivity of colloidal ferric iron nanoparticles cannot be expected a priori. The column-scale experiment is therefore suggested to gain insight into the environmental relevance of nanosized iron (hydr)oxides in microbial reduction, at the example of ferrihydrite colloids.

MATERIAL AND METHODS

Columns

Stainless steel columns with an inner diameter of 35 mm and a height of 250 mm (volume = 240 cm^3) were used as experimental microcosms. Both ends of the columns were capped with stainless steel caps, a stainless steel dispenser-layer integrated in the column cap (pore size ~1 mm), and operated under water-saturated conditions in bottom-to-top flow mode. Prior to saturation, the columns were homogenously filled to uniform bulk density of 1.8 g cm^{-3} with either goethite-coated quartz-sand (column 1 and 3, pore volume = 92.5 ml) or pure quartz sand without goethite coatings (column 2, pore volume = 92.2 ml), respectively. Quartz sand (Carl Roth, Karlsruhe, Germany) with a grain size of 0.4 – 0.8 mm was applied as basic matrix and used as model system for a porous medium. The material was thoroughly washed with MilliQ-water and heated for 24 h at 800°C. The quartz-sand was coated with goethite as described before (Foppen et al. 2006). Goethite was obtained from Sigma (Deisenhofen, Germany) and the mineral structure was confirmed by X-ray diffraction (Figure 1). The total Fe content of the goethite-coated quartz sand was 11.8 μmol Fe (g sand)$^{-1}$. No iron could be detected in the uncoated quartz sand. The complete setup was installed in an anoxic, nitrogen-atmosphere glove-box (O_2-content < 3 ppm) at 25.1 ± 2.6°C.

The mineral medium was introduced using stainless steel fittings, Fluran tubings, and an IPC Multichannel Dispenser (Ismatec, Wertheim, Germany). The flow rate was set to 1.75 ml h^{-1}, which equals to a pore water velocity υ of 0.49 cm h^{-1} and an exchange of 0.5 pore volumes (PV) per day. Prior to the experiment, the columns were saturated at very low flow velocity (~0.6 ml h^{-1}) from bottom to top using 1 mM NaCl solution to remove all entrapped air from the porous matrix.

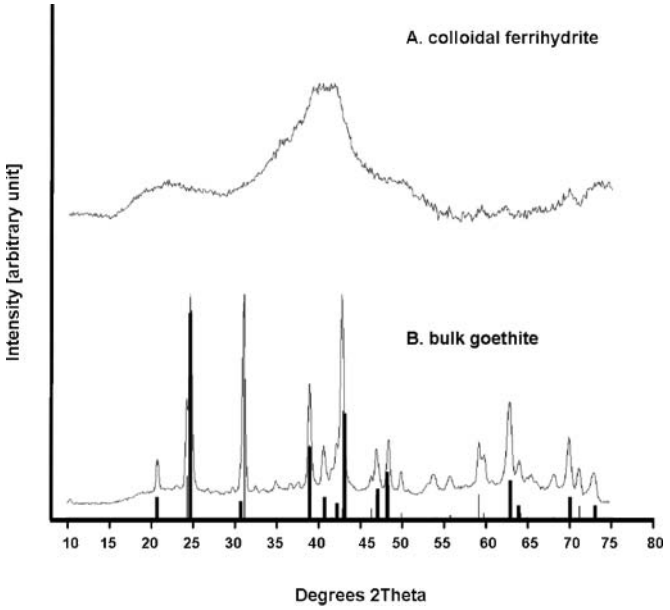

FIG. 1. XRD patterns of the iron oxides used in the column experiment. A: XRD-pattern for 336 nm colloidal ferrihydrite. The synthesized mineral was amorphous, due to small particle size. The material can nevertheless be roughly identified as ferrihydrite by comparison with typical ferrihydrite patterns which show clustered peaks between 18 to 45°2 Theta (e.g., PDF-4 No. 01-72-76731 or PDF-4 No. 00-46-1351). B: bulk goethite as indicated by reference pattern PDF No. 29-0713 for goethite (black bars). The mineral was identified as pure, well-crystalline goethite, with a minor contamination of quartz particles (PDF No. 33-1161, thin grey bars). The intensities of A and B are not plotted on the same y-axis.

A conservative tracer breakthrough experiment was performed using 1 mM Bromide which was analysed by ion chromatography (Dionex DX-120, AG4A-SC+AS4A-SC, 1.7 mM $NaHCO_3$ + 1.8 mM Na_2CO_3). The breakthrough curves were analysed by fitting the advection-dispersion equation (CXTFit, Toride et al., 1999). The retardation coefficient R ranged within the interval R = 1.059–1.088 (σ = 0.003) which implies the non-retardation of bromide transport. In conclusion, bromide qualified as conservative tracer in this study. The breakthrough demonstrated the homogeneous fillings of the columns and the non-existence of preferential flow-paths (Figure 2).

Microorganism and Cultivation

Geobacter sulfurreducens DSMZ 12127 (Caccavo et al. 1994) was obtained from the German Collection of Microorganisms and Cell Cultures (Braunschweig, Germany). The strain was cultivated on 50 mM ferric citrate as terminal electron acceptor at 30°C in the dark using standard anaerobic techniques. Sodium acetate (10.0 ± 1.0 mM) was added as sole energy and carbon source.

Autoclaved, anoxic low salt mineral medium was used throughout the study as column influent, consisting of 100 mg L^{-1} NaCl, 4 mg L^{-1} $MgCl_2 \cdot 6H_2O$, 25 mg L^{-1} NH_4Cl, 50 mg

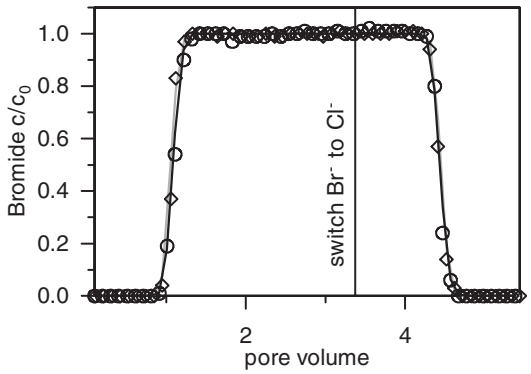

FIG. 2. Breakthrough of Br^- as conservative tracer at a pore water veolocity of $\upsilon = 0.98$ cm h^{-1}(= 1 PV d^{-1}). c = effluent concentration; c_0 = influent concentration; C1 = Column 1: Observed (○), Column 1: Fitted (black line), C2 = Column 2: Observed (◇), Column 2: Fitted (grey line).

L^{-1} KCl, 1.5 mg L^{-1} $CaCl_2 \cdot 2H_2O$, and 10.0 ± 1.0 mM sodium acetate as electron and carbon donor. Phosphate was omitted to avoid interactions with iron oxide surfaces. This mineral medium was supplemented with 10-fold diluted trace elements solution SL10 (Widdel et al. 1983), selenite-tungsten, and vitamins solutions (Widdel and Pfennig 1981). As a sulfur source, 10 μM Na_2SO_4 was added. Heat-sensitive components were added via 0.22 μm filtration. The medium was buffered with 10 mM Tris/HCl at pH 7.0. As a general stimulating agent for anaerobic growth, cAMP was added at 10 μM. All chemicals were at least ACS grade.

Synthesis and Characterization of Colloidal Ferrihydrite

Colloidal iron hydroxide was produced as described in Leibl et al. (1999). Initially, 4.19 g of ferric citrate were dissolved in 100 ml MilliQ-water, and the pH was adjusted with 10 N NaOH under vigorous stirring to pH 8. Stirring was maintained for 30 min. The resulting ferrihydrite colloids were concentrated by several cycles of centrifugation and resuspension in MilliQ-water until the total carbon content in the supernatant dropped below 1 mg L^{-1}. The colloids had a hydrodynamic diameter of 336 nm determined by dynamic light scattering (DLS, see below) with a surface area of 275 ± 0.6 m^2 g^{-1} as confirmed by Brunauer-Emmet-Teller N_2-physisorption (BET) measurements (Brunauer et al. 1938). The mineral was indicated to be ferrihydrite by XRD (Figure 1). The colloidal iron hydroxide solution had a Fe(III) content of 8.8 mM, and was added to the columns together with the mineral medium in a 50/50 ratio.

Experimental Procedure and Analysis

To test the reactivity of iron oxide colloids under flow conditions in a porous medium, three different species of Fe(III) were applied as electron acceptor to three different experimental columns: bulk, crystalline goethite as coating on the porous matrix (C1), ferrihydrite colloids (C2), and a combination of both (C3). The porous matrix, low initial influent cell densities, and the applied flow regime in the column experiments were designed to approach in situ conditions in (groundwater) aquifers.

After saturation with MilliQ-water containing 1 mM NaCl, the columns were flushed for 9 PV with the mineral medium to ensure chemical equilibrium and removal of any residual particulate matter. The subsequent experimental phases were: (i) inoculation of the columns with diluted pre-culture bacteria for altogether 38 PV at different intervals (see Figure 3), (ii) colonization of the porous medium, and (iii) application of ferrihydrite colloids at a concentration of 4.4 mM. *Geobacter sulfurreducens* cells were added to the influent medium reservoir and inoculation of the columns took place via the influent at a concentration of 2.5 × 10^4 cells ml^{-1}. The application of iron hydroxide colloids was performed via a parallel reservoir, so that no iron reduction could occur outside the columns. Over

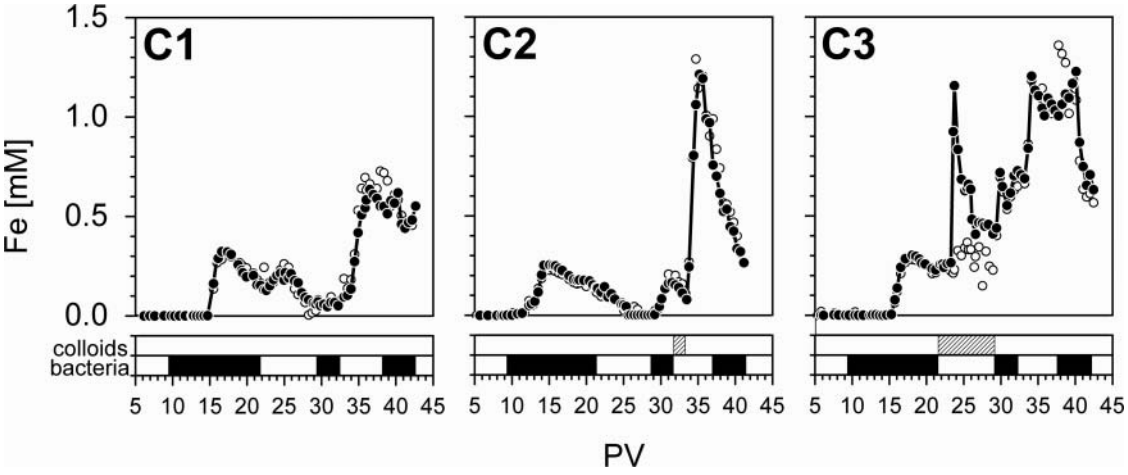

FIG. 3. Fe^{2+} (○) and total Fe (●) discharge from continuous-flow sand columns inoculated with *Geobacter sulfurreducens*. Different forms of ferric iron were applied in the columns. C1: goethite-coated quartz sand. C2: ferrihydrite colloids introduced via the influent, no goethite-coatings. C3: goethite-coated quartz sand and introduced ferrihydrite colloids. Black bars: periods of microorganism inoculation. Hatched bars: periods of colloidal ferrihydrite input. PV = pore volume.

the course of the experiment, Fe^{2+}, total Fe, pH, redox (measured against normal hydrogen electrode), and particle size distributions were permanently assessed in the effluent. After the experiment the content and spatial distribution of iron in the porous medium was assessed by sampling three layers of quartz sand in each column under anoxic conditions. The bottom, middle and top layers were analyzed for total as well as for ferrous iron content.

Iron reduction was analyzed by measuring Fe^{2+} concentrations using the ferrozine assay (Stookey 1970). Aliquots of 0.1 ml were diluted 1:10 in 1 M HCL and shaken at 1400 rpm for 24 h to remove all adsorbed Fe^{2+} from solid iron oxide surfaces. Subsequently, ferrozine was added. Absorbance was measured at 560 nm. Total iron was analyzed by addition of 32% HCl (Merck, Germany) to the effluent samples to achieve a final amount of 1 M HCl in the samples. The samples were shaken overnight to ensure complete dissolution of particulate iron hydroxides. Total Fe was then estimated by ICP-OES (Vista Pro, Varian Inc., USA). The total iron of the solid phase material was extracted with a dithionite-citrate-bicarbonate solution (Mehra and Jackson 1960). Overall iron amounts in the effluent were obtained by integrating concentrations over time.

Particle size distribution of the colloidal iron oxide in the influent and effluent was estimated by dynamic light scattering (DLS). A ZetaSizer Nano ZS and a HPPS 5001 (both Malvern Instruments, Worcestershire, UK) were used with low volume sizing cuvettes. At least triplicate measurements of 30 sec each were taken. Calibration latex beads 80 nm in size were measured to confirm the accuracy of the method.

Flow-cytometry was applied to count cells in the effluent using a LSRII (Becton Dickson Bioscience, Franklin Lakes, NJ, USA). The samples were fixed with paraformaldehyde, stained by SYBR® Green I nucleic acid stain (Molecular Probes, Eugene, OR, USA), diluted in 0.22 μm-filtered Dulbecco's-PBS, thoroughly vortexed and counted at a wavelength of 510 nm in Trucount™ bead (Becton Dickson) calibrated measurements.

RESULTS AND DISCUSSION

Microbial Iron Reduction of the Goethite-Coating

To analyze the reduction of goethite by *Geobacter sulfurreducens* under flow conditions in a porous matrix, column 1 (C1) was operated with goethite-coated quartz sand as terminal electron acceptor. After the first inoculation with *G. sulfurreducens* at pore volume (PV) 9, no iron reduction could be observed (Figure 3). According to the tracer breakthrough (Figure 2), residual Fe^{2+} from the influent medium of the *Geobacter* cell suspension (0.2 mM Fe^{2+}) should have appeared in the effluent ≈1 PV after input. This breakthrough was retarded though, possibly by an initial adsorption of Fe^{2+} at the goethite matrix as has been observed previously (Roden 2000).

Then, the concentration of total iron in the effluent increased to 0.3 mM which was released completely as Fe^{2+}. This was only slightly elevated compared to the Fe^{2+} content of the influent medium introduced by the *Geobacter* cell suspension. Obviously, only little iron reduction occurred in C1 after the initial inoculation with *G. sulfurreducens*. This was also observed in the parallel columns C2 and C3 (Figure 3). We attribute the initially limited Fe(III) reduction to the still high redox potentials of around 0 to −50 mV measured in the effluent (Figure 4), which might have inhibited *Geobacter*. However, the redox potential dropped to around −250 mV after PV 13, indicating an ongoing, probably biotic modification of the redox environment within the columns, yet without a visible increase of iron reduction. Only after PV 30, an increase in Fe^{2+} release due to microbial iron reduction could be observed, with Fe^{2+} concentrations in the effluent of C1 rising to 0.6 mM. Altogether, a net amount (having already subtracted the inflow) of 0.5 mmol Fe^{2+} was released from the column. The same amount of Fe(III) must have been depleted from the goethite within C1, as there was no other Fe(III) source. This equals to a 10% reduction of the initial Fe(III) within C1 (4.8 mmol; Table 1), and indicated the low bioavailability of the highly crystalline goethite coating.

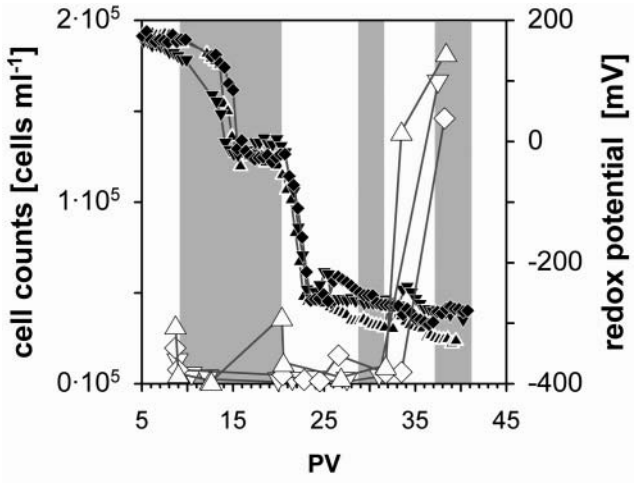

FIG. 4. Cell counts in the effluent and redox potentials in the experimental columns over the course of the experiment. Redox potential of column 1 (▲), column 2 (▼), and column 3 (♦) are shown as closed symbols, cell counts are shown as respective open symbols. Grey background bars denote periods of bacterial inoculation.

Dithionite-extraction of Fe from the goethite-coated quartz sand in C1 after the experiment could not match to all residual ferric iron from the column matrix. We expected a depletion of 0.5 mmol iron according to the measured discharge of ferrous iron (Figure 3), but found a depletion of 1.7 mmol as indicated by the profile samples (Figure 5). We explain this overestimation as an error due to the heterogeneous iron distribution in C1 (strong adsorption within the first 5 cm of the column) and large spatial sampling intervals along the column profile.

Based on the effluent data, the detected microbial reduction equaled to 1.2 μmol Fe^{2+} (g sand)$^{-1}$ released from the initial goethite concentration of 11.8 μmol g^{-1}. A strong depletion of Fe(III) in the lower third of the column (inflow) was observed,

TABLE 1
Electron balance of microbial iron reduction in columns with different iron oxides as terminal electron acceptors for *Geobacter sulfurreducens*

	Pre-experimental		Post-experimental		e-balance
[mmol]	influent	column interior		effluent	[net $\triangle Fe^{2+}$ vs. net $\triangle$Fe(III)]
C1					
Fe^{2+}	0.5	0.0	0.2	0.8	+0.5
Fe(III)	0.0	4.8 goethite	3.2	0.0	–1.7[a]
C2					
Fe^{2+}	0.5	0.0	0.1	0.8	+ 0.4
Fe(III)	0.6 colloids	0.0	0.2	0.0	–0.4
C3					
Fe^{2+}	0.5	0.0	0.4	1.5	+ 1.4
Fe(III)	2.6 colloids	4.8 goethite	5.8	0.2	–1.4

[a]Fe(III) from the column interior after the experiment could no be fully retrieved. See discussion. Data give the overall content of Fe^{2+} and Fe(III) in the influent, inside the column prior to the experiment, after the experiment, and in the effluent (all data in mmol). Available electron acceptors: C1: goethite-coated quartz sand inside column. C2: colloidal ferrihydrite applied via influent, no goethite-coatings. C3: goethite-coated quartz sand plus colloidal ferrihydrite applied via the influent.

indicating a hotspot of microbial reduction (Figure 5). In agreement with this finding, previous studies showed in comparable experiments, that the highest microbial activity was close to the inlet (von Gunten and Zobrist 1993; Thullner 2005).

Hence, this can be assumed to be the maximum iron reduction capacity of goethite-coated quartz sand in this experimental setup. The cumulative rate of iron reduction in C1 was at 0.02 μmol $Fe^{2+}g^{-1}$ d^{-1}. A rate of 0.54 μmol Fe^{2+} g^{-1} d^{-1} was calculated from the data by Roden et al. (2000). We applied a low salt mineral medium at roughly 1:10 the ionic strength of common growth media. This ensured the stability of the applied ferrihydrite colloids within the other experimental column C2, but probably diminished microbial growth. Additionally, the study of Roden (2000) used around 10-fold higher ferric iron concentrations, which might be another reason for the lower rates observed in our study. Ferric iron was not released from column C1, indicating the overall structural integrity of the goethite matrix at neutral pH.

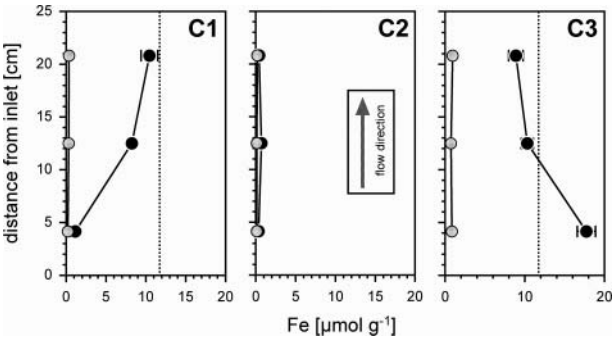

FIG. 5. Fe^{2+} (○) and total Fe (●) content of the column matrix after the experiment. C1 (goethite-coated quartz sand only), C2 (colloidal ferrihydrite input, quartz sand without goethite-coating,) and C3 (goethite-coated quartz sand plus colloidal ferrihydrite input). The dashed line equals to the initial total Fe-content of the goethite-coated quartz sand. Error bars denote standard deviation of triplicate samples.

Microbial Reduction of Colloidal Ferrihydrite

Column 2 (C2), containing uncoated quartz-sand only, showed no iron reduction upon the first inoculation with *G. sulfurreducens* as no terminal electron acceptor was available. The effluent iron discharge (0.2 to 0.3 mM) in the early stage of the experiment stemmed from the inoculum input via the influent as observed identically in C1 and C3. After adding ferrihydrite colloids for 1.4 PVs to the influent, a rapid response was observed (Figure 3): The effluent Fe^{2+} increased very rapidly to 1.2 mM immediately after application. A total amount of 0.4 mmol Fe^{2+} was released by C2. During this time, 0.6 mmol Fe(III) were introduced as ferrihydrite colloids into C2, indicating that 66 % of the introduced nanoparticles were microbially reduced. Compared to the degree of reduction of the goethite coating in C1 (10%), and also compared to the degree of reduction of other bulk ferric oxides under batch conditions (Roden 1996), this is strikingly high. The remaining minor fraction of the iron oxide colloids was retained inside C2 (Table 1), most likely by adsorption, and was retrieved after the experiment from the quartz sand matrix (Figure 5).

Obviously, transport of Fe^{2+} through C2 was retarded to a much lesser extent than observed in C1. Inoculation at PV 29 and the associated introduction of Fe^{2+} via the cell suspension showed even no retarded transport (Figure 3). These observations are attributed to the lack of goethite-coatings which serve as adsorption matrix for Fe^{2+} and delay its discharge from the column. This implies that a delay in Fe^{2+}-discharge in C1 and

C3 (goethite-coated quartz sand) is caused by adsorption of Fe^{2+} to the bulk phase.

Microbial Reduction of Goethite-Coating in Combination with Colloidal Ferrihydrite

When the goethite-coated sand of column 3 (C3) was flushed with the *Geobacter* inoculum, C3 reacted similar to C1. Fe^{2+} transport through the column was retarded and Fe^{2+} concentrations of the effluent were only slightly higher than the influent background (Figure 3). In contrast to Fe^{2+}, added ferrihydrite colloids (PV 22) were rapidly transported through the column matrix and were detected in the effluent as Fe(III) after ~1 exchanged PV. This is comparable to the speed of a conservative tracer (Figure 2), thus excluding size-exclusions effects on the transport of the 336 nm colloids through the porous medium used in this study (medium sized and coarse sand). Yet, almost no increase of Fe^{2+} as an indicator for enhanced microbial iron reduction was measured in the effluent. Instead, the appearance of 0.9 mM Fe(III) in the effluent suggests the breakthrough of unreduced iron oxide colloids. The particle size measurements in the effluent matched this breakthrough, as particles with a diameter of ~300 nm were detected equalling the size of the introduced ferrihydrite colloids (Data not shown).

The presence of colloids in the effluent soon diminished after the initial breakthrough, indicating either a strong retardation or reduction of the colloids within the matrix. The solid phase extraction of Fe in C3 after the experiment indicated a deposition of colloids at the column inlet (Figure 5). So, we assume a partial retardation of colloids by interaction with the porous medium, whereas a significant portion of colloids is transported through the column similar to a conservative tracer, though.

After PV 24, Fe^{2+} concentration in the discharge remained initially constant, and then began to rise steadily for 16 PV, even after the colloid input was stopped. After PV 29, when inoculation with *G. sulfurreducens* restarted, microbial iron reduction increased strongly to Fe^{2+} concentrations of 1.2 mM. Hence, an elongated and sustained microbial reduction of the adsorbed colloids on the goethite matrix took place.

Until the end of the experiment in C3, 2.6 mmol Fe(III) were introduced as ferrihydrite colloids, while 0.2 mmol of colloidal Fe(III) were detected in the effluent (Table 1). Thus, 2.4 mmol of the colloids remained within the column and were subject either to adsorption to the goethite matrix or microbial reduction. Between PV 5 and 45, altogether 1.4 mmol of Fe^{2+} were generated within C3, at a cumulative rate of 0.05 μmol g^{-1} d^{-1} which is twice the rate of iron reduction in C1. Fe(III) within C3 increased from 4.8 mmol Fe to 5.8 mmol, indicating that at least 1.0 mmol or 38% of the introduced iron oxide colloids were retained by the matrix (Table 1). Subtracting the amount of retained (1.0 mmol) and discharged colloids (0.2 mmol) from the influent colloids (2.6 mmol) indicated that 54% of the introduced iron oxide colloids were reduced within the column, though a partial reduction of the goethite matrix cannot be ruled out.

As a control for abiotic iron reduction, mixtures of the goethite-coated quartz sand, mineral medium, ferrihydrite colloids and the 0.22 μm-filtered bacterial cell suspension were incubated under batch conditions, but no iron reduction was observed here (data not shown).

High Reactivity of Colloidal Iron Oxide

The colloidal iron hydroxide applied to C2 and C3 were readily reduced, even though they were adsorbed to the matrix in C3. C2 and C3 show double concentrations of effluent Fe^{2+} compared to C1, and a high degree of reduction of the colloidal Fe(III) of 66% and 54%, respectively (calculated from the net decrease of Fe(III) to the introduced Fe(III), see Table 1). Interestingly, the strong retention of iron oxide colloids to the goethite coating in C3 led to an elongated reduction as compared to C2, where most of the introduced colloids were reduced within ~5 PV. This delayed reaction led in turn to elevated reduction rates over a longer time span. Elevated Fe^{2+} production in C3 lasted for at least ~15 PV and the reduction was still ongoing at the end of the experiment indicating the high bioavailability of deposited iron colloids.

Our findings constitute one step forward towards the understanding of the role of colloidal iron oxides in microbial iron reduction in water-saturated porous environments. In porous media, colloidal iron oxides seem to be very reactive even when adsorbed to the matrix. The high reactivity observed in C2 and C3 can only be attributed to the addition of ferrihydrite colloids, as this was the only distinguishing feature compared to C1.

Ferric oxide nanoparticles seem as a feasible agent of bioremediation in this respect, as they enhance microbial iron reduction not only while being suspended, but also as an adsorbed, reactive electron acceptor pool over a longer time-span.

Environmental Implications

Natural sediments represent a heterogeneous size distribution of pore spaces and spatially varying compositions of reactive surfaces, leading to a transport behavior of added iron oxide colloids controlled by concurring adsorption and remobilization processes (Kretzschmar and Sticher 1997; Bunn et al. 2002; McCarthy and McKay 2004). Secondary mineralization and transformations of ferric oxides will have a stronger impact (Hansel et al. 2003; Hansel et al. 2004; Pedersen et al. 2005), as well as pH-dependent aggregation (He et al. 2008) and the impact of humic substances on colloid stability (Bauer and Blodau 2009; Yang et al. 2009).

Nevertheless, colloid-mediated microbial iron reduction now can be suggested as a viable mechanism in the environment. Ferrihydrite colloids showed their high intrinsic reactivity and bioavailability which so far were observed only in static batch tests, also under flow conditions and adsorbed to a porous matrix. Flow velocity variations and the heterogeneous pore size distribution are suggested as crucial parameters determining either the complete reductive dissolution of iron oxide colloids

and associated compounds or the export from the system. Reactive amorphous iron oxides in aquifers are known to be abundant in aquifer sediments (Swartz et al. 1997).

Our findings add a microbial perspective to this picture in a way that high iron turnover rates for anoxic aquifers now become reasonable to be considered. Of course, high reduction rates of amorphous iron oxides in aquifer sediments have been reported before, and they have been contrasted by the low reactivity of crystalline iron oxides (Roden and Urrutia 2002). Nevertheless, nanosized iron oxides in colloidal suspension constitute a putative subset of the amorphous ferric iron fraction in aquifer sediments with high reactivity comparable to regular hydrous ferric oxide coatings. The possible origins of colloidal ferric oxides in an aquifer might be the oxidation of ferrous iron at transition zones, conceivably at, e.g., plume fringes, or weathering reactions of mineral surfaces. Apart from the occurrence of naturally formed iron oxide colloids, an application of synthesized material for remediation purposes seems feasible.

In summary, mobile colloidal iron hydroxides are likely to be reduced much faster than bulk crystalline Fe(III) oxide grain coatings, and may comprise a significant source of bioavailable Fe(III) oxide input to aquifer sediments.

REFERENCES

Anschutz AJ, Penn RL. 2005. Reduction of crystalline iron(III) oxyhydroxides using hydroquinone: Influence of phase and particle size. Geochem Trans 6:60–66.

Bauer M, Blodau C. 2009. Arsenic distribution in the dissolved, colloidal and particulate size fraction of experimental solutions rich in dissolved organic matter and ferric iron. Geochim Cosmochim Acta 73: 529–542.

Bosch J, Heister K, Hofmann T, Meckenstock RU. 2010. Nanosized iron oxide colloids strongly enhance microbial iron reduction. Appl Environ Micobiol 7:184–189.

Bose S, Hochella Jr MF, Gorby YA, Kennedy DW, McCready DE, Madden AS, Lower BH. 2009. Bioreduction of hematite nanoparticles by the dissimilatory iron reducing bacterium *Shewanella oneidensis* MR-1. Geochim Cosmochim Acta 73: 962–976.

Brunauer S, Emmett PH, Teller E. 1938. Adsorption of gases in multimolecular layers. J Am Chem Soc 60:309–319.

Bunn RA, Magelky RD, Ryan JN, Elimelech M. 2002. Mobilization of natural colloids from an iron oxide-coated sand aquifer: Effect of pH and ionic strength. Environ Sci Technol 36:314–322.

Caccavo F, Lonergan DJ, Lovley DR, Davis M, Stolz JF, McInerney MJ. 1994. *Geobacter sulfurreducens* sp. nov., a hydrogen- and acetate oxidizing dissimilatory metal-reducing microorganism. Appl Environ Microbiol 60:3752–3759.

Foppen JWA, Okletey, S., Schijven, J.F. 2006. Effect of goethite coating and humic acid on the transport of bacteriophage PRD1 in columns of sturated sand. J Contam Hydrol 85:287–301.

Gilbert B, Banfield JF. 2005. Molecular-scale processes involving nanoparticulate minerals in biogeochemical systems. Rev Mineral Geochem 59:109–155.

Hansel CM, Benner SG, Neiss J, Dohnalkova A, Kukkadapu RK, Fendorf S. 2003. Secondary mineralization pathways induced by dissimilatory iron reduction of ferrihydrite under advective flow. Geochim Cosmochim Acta 67:2977–2992.

Hansel CM, Benner SG, Nico P, Fendorf S. 2004. Structural constraints of ferric (hydr)oxides on dissimilatory iron reduction and the fate of Fe(II). Geochim Cosmochim Acta 68:3217–3229.

He YT, Wan JM, Tokunaga T. 2008. Kinetic stability of hematite nanoparticles: the effect of particle sizes. J Nanopart Res 10:321–332.

Hochella MF, Lower SK, Maurice PA, Penn RL, Sahai N, Sparks DL, Twining BS. 2008. Nanominerals, mineral nanoparticles, and Earth systems. Science 319:1631–1635.

Kerisit S, Rosso KM, Dupuis M, Valiev M. 2007. Molecular computational investigation of electron-transfer kinetics across cytochrome-iron oxide interfaces. J Phys Chem C 111:11363–11375.

Kretzschmar R, Robarge WP, Amoozegar A. 1995. Influence of Natural Organic Matter On Colloid Transport Through Saprolite. Water Resour Res 31:435–445.

Kretzschmar R, Sticher H. 1997. Transport of humic-coated iron oxide colloids in a sandy soil: Influence of Ca2+ and trace metals. Environ Sci Technol 31:3497–3504.

Leibl H, Tomasits R, Bruhl P, Kerschbaum S, Eibl MM, Mannhalter JW. 1999. Humoral and cellular immunity induced by antigens adjuvanted with colloidal iron hydroxide. Vaccine 17:1017–1023.

McCarthy JF, McKay LD. 2004. Colloid transport in the subsurface: past, present and future challenges. Vad Zone J 3:326–337.

Mehra OP, Jackson ML 1960. Iron oxide removal from soils and clays by a dithionite-citrate system buffered with sodium carbonate. In: Proceedings of the 7th National Conference on Clays and Clay Minerals (ed Ingerson E). Pergamon Press, London. P317–327.

Pedersen HD, Postma D, Jakobsen R, Larsen O. 2005. Fast transformation of iron oxyhydroxides by the catalytic action of aqueous Fe(II). Geochim Cosmochim Acta 69:3967–3977.

Roden EE. 2000. Bacterial reductive dissolution of crystalline Fe(III) oxide in continuous-flow column reactors. Appl Environ Microbiol 66:1062–1065.

Roden EE, Urrutia MM. 2002. Influence of Biogenic Fe(II) on Bacterial Crystalline Fe(III) Oxide Reduction. Geomicrobiol J 19:209–251.

Roden EE, Zachara, JM. 1996. Microbial reduction of crystalline iron(III) oxides: Influence of oxide surface area and potential for cell growth. Environ Sci Technol 30:1618–1628.

Stookey LL. 1970. Ferrozine—A new spectrophotometric reagent for iron. Anal Chem 42:779–781.

Swartz CH, Ulery AL, Gschwend PM. 1997. An AEM-TEM study of nanometer-scale mineral associations in an aquifer sand: Implications for colloid mobilization. Geochim Cosmochim Acta 61:707–718.

Thullner M. 2005. Modeling the impact of microbial activity on redox dynamics in porous media. Geochim Cosmochim Acta 69:5005–5019.

van der Zee C. 2003. Nanogoethite is the dominant reactive oxyhydroxide phase in lake and marine sediments. Geology 31:993–996.

von Gunten U, Zobrist J. 1993. Biogeochemical changes in groundwater-infiltration systems: Column studies. Geochim Cosmochim Acta 57:3895–3906.

Waychunas GA, Kim CS, Banfield JF. 2005. Nanoparticulate iron oxide minerals in soils and sediments: unique properties and contaminant scavenging mechanisms. J Nanopart Res 7:409–433.

Widdel F, Kohring GW, Mayer F. 1983. Studies in dissimilatory sulfate-reducing bacteria that decompose fatty acids. III. Characterization of the filamentous gliding *Desulfonema limicola* ge. nov. sp. nov., and *Desulfonema magnum* sp. nov. Arch Microbiol 134:286–294.

Widdel F, Pfennig N. 1981. Studies in dissimilatory sulfate-reducing bacteria that decompose fatty acids. III. Isolation of a new sulfate-reducer enriched with acetate from saline environments. Description of *Desulfobacter postgatei* gen. nov. sp. nov. Arch Microbiol 129:395–400.

Yan B, Wrenn BA, Basak S, Biswas P, Giammar DE. 2008. Microbial reduction of Fe(III) in hematite nanoparticles by Geobacter sulfurreducens. Environ Sci Technol 42:6526–6531.

Yang K, Daohui L, BXing B. 2009. Interactions of Humic Acids with nanosized Inorganic Oxides. Langmuir 25:3571–3576.